Growth of graphene on Ir(111)

New Journal of Physics
The open-access journal for physics

Growth of graphene on Ir(111)

Johann Coraux [1,4], Alpha T N'Diaye[1,5], Martin Engler[1], Carsten Busse[1], Dirk Wall[2], Niemma Buckanie[2], Frank-J Meyer zu Heringdorf[2], Raoul van Gastel[3], Bene Poelsema[3] and Thomas Michely[1]

[1] II. Physikalisches Institut, Universität zu Köln, Zülpicher Straße 77, 50937 Köln, Germany
[2] Institut für Experimentelle Physik, Universität Duisburg–Essen, Lotharstrasse 1, 47057 Duisburg, Germany
[3] MESA+ Institute for Nanotechnology, University of Twente, PO Box 217, 7500 AE Enschede, The Netherlands
E-mail: ndiaye@ph2.uni-koeln.de

New Journal of Physics **11** (2009) 023006 (22pp)
Received 29 October 2008
Published 4 February 2009
Online at http://www.njp.org/
doi:10.1088/1367-2630/11/2/023006

Abstract. Catalytic decomposition of hydrocarbons on transition metals attracts a renewed interest as a route toward high-quality graphene prepared in a reproducible manner. Here we employ two growth methods for graphene on Ir(111), namely room temperature adsorption and thermal decomposition at 870–1470 K (temperature programmed growth (TPG)) as well as direct exposure of the hot substrate at 870–1320 K (chemical vapor deposition (CVD)). The temperature- and exposure-dependent growth of graphene is investigated in detail by scanning tunneling microscopy. TPG is found to yield compact graphene islands bounded by C zigzag edges. The island size may be tuned from a few to a couple of tens of nanometers through Smoluchowski ripening. In the CVD growth, the carbon in ethene molecules arriving on the Ir surface is found to convert with probability near unity to graphene. The temperature-dependent nucleation, interaction with steps and coalescence of graphene islands are analyzed and a consistent model for CVD growth is developed.

[4] Permanent address: Institut Néel/CNRS, 25 rue des Martyrs, BP 166, 38042 Grenoble cedex 9, France.
[5] Author to whom any correspondence should be addressed.

Contents

1. Introduction

Intense research on the electronic properties of graphene was initiated in 2004 using both exfoliated [1] and epitaxial [2] graphenes. From then on, theoretical and experimental efforts allowed one to unravel some of the unique physical properties of graphene [3, 4].

Although most of the experimental research on graphene still relies on exfoliated graphene, the route toward practical realization calls for reproducible methods for the production of high-quality graphene single layers with macroscopic extension. In this respect, epitaxial graphene on a silicon carbide (SiC) substrate has attracted much interest. Whatever the recent progress in the preparation of graphene/SiC, the charge carrier mobilities remain comparable to the first ones reported [2, 5, 6], and much lower than for exfoliated graphene [7]. Whether these reduced mobilities originate from structural defects in the graphene layer itself or in the buffer layer between the SiC substrate and the graphene layer has not yet been elucidated. Additionally, the growth of a well-defined number of graphene layers on SiC appears to be a major difficulty, as a mixture of mono-, bi-, tri-, etc, layers with distinct physical properties is usually obtained. Graphene growth on dense packed surfaces of transition metals—well known already for several decades [8]—is currently receiving renewed interest. Indeed, graphene growth catalyzed by the metallic surface is self-limited to a single layer, and high structural quality can be achieved, as recently shown for graphene on Ir(111) [9]. A further step towards applications could involve the transfer of such graphene layers onto a nonconducting substrate [3, 10].

The graphene/metal interface is a model system, where interaction between graphene π-bands and the metal bands can be investigated. This has relevance for contacting graphene with metal electrodes. The carbon hybridization or the epitaxial relationship with the metal was proposed to influence the contact transmittance [11, 12] or cause local doping of graphene [13, 14]. A variety of situations are realized depending on the support material, from almost no interaction in the case of Ir(111) [15], to a deep modification of the electronic structure in the case of a graphene monolayer on Ni(111) [16, 17] or Ru(0001) [18, 19]. Other fundamental questions come along with the metal/graphene interface, in particular, considering supercurrent with Dirac-like electrons flowing between two metallic electrodes coupled through a graphene layer to a superconductor [20]. With respect to spintronics, recent work focusing on

spin filtering highlighted the relevance of epitaxial graphene on a ferromagnetic metal, like Ni or Co [21]–[23].

Numerous metallic surfaces were employed for the growth of epitaxial graphene [8], including Ir(111) [9], [24]–[28] which is of interest in the present article. A growing number of experimental investigations make use of local probes and their capability to efficiently investigate the structure and growth of graphene, i.e. the shape and extension of graphene as well as the occurrence of superstructures or defects. Examples include studies of graphene on Pt(111) [29, 30], Ni(111) [16, 21, 22] Ir(111) [9, 27, 28, 31], and Ru(0001) [19, 32, 33]. Here, we provide an analysis of the growth of graphene on Ir(111), based on scanning tunneling microscopy (STM). The motivation of the work reported below was threefold: (i) understanding the growth mechanisms, (ii) settling procedures for the achievement of high structural quality graphene and (iii) tailoring the morphology of graphene, from large continuous flakes to small graphene islands.

2. Experimental

Experiments were performed in an ultrahigh vacuum (UHV) chamber with base pressure in the 10^{-11} mbar range. The sample surface was prepared by repeated cycles of sputtering at 1120 K followed by an annealing step at 1570 K, yielding clean Ir(111) exhibiting terraces extending over several hundreds of nanometers. The growth of graphene was performed using the decomposition of carbon-containing molecules, especially ethene (C_2H_4), which is catalyzed by the Ir substrate. Two growth methods were employed. The first one, consisting of room temperature adsorption of the molecules followed by pyrolysis and graphene growth at a fixed elevated temperature, will in the following be referred to as temperature programmed growth (TPG). As a second growth method, chemical vapor deposition (CVD) of ethene on a hot Ir surface was employed. Ethene was provided through a 7 mm diameter dosing tube, which ends 2 cm away from the sample surface. In the following, we always specify the pressure measured away from the sample surface, with an ion gauge distant from the doser. The local ethene partial pressure at the sample surface was assessed to be 80 ± 20 times higher than the measured pressure (not taking into account any correction factor for the ion gauge). This factor was determined by exposing the sample to the ethene flux for a short time at a fixed ethylene partial pressure and subsequent TPG. The coverage with graphene was then related to the ethene dose. As no carbon desorbs during heating [34], this allows one to infer the local pressure at the sample surface.

TPG with coronene ($C_{24}H_{12}$), which is a polycyclic aromatic hydrocarbon consisting of seven carbon rings, was also performed. Coronene was provided by a homemade evaporator.

3. TPG

3.1. Results

By STM, we observed the carbon precipitation after TPG using a heating interval of 20 s at varying temperatures. Carbon islands grown by an 870 K TPG step (figure 1(a)) have a typical diameter of less than 2 nm and vary in height. In contrast to this, TPG at 970 K (figure 1(b)) leads to the formation of flat islands that have a well-defined height and straight edges. From this temperature on the islands exhibit a typical moiré superstructure [9, 27, 28]. The moiré structure

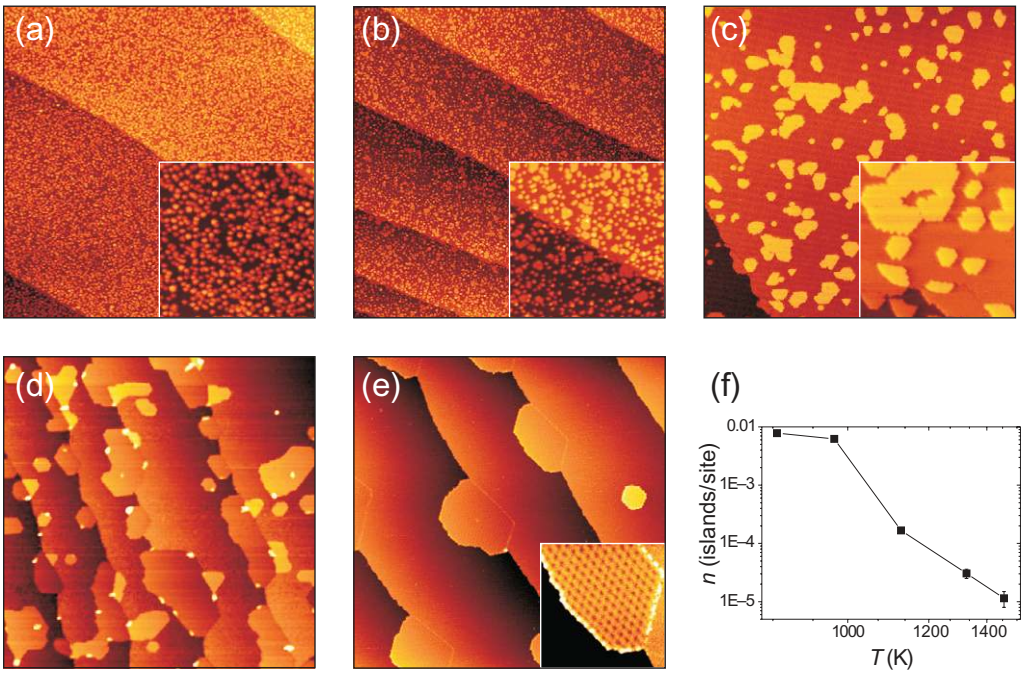

Figure 1. STM topographs (250 nm × 250 nm; insets (a)–(c) 62 nm × 62 nm, inset (e) 40 nm × 40 nm) of graphene prepared along the TPG procedure, after annealing for 20 s to (a) 870 K, (b) 970 K, (c) 1120 K, (d) 1320 K and (e) 1470 K. (f) Density n of graphene islands as a function of the annealing temperature T in the TPG.

can be resolved for low tunneling resistances (see inset of figure 1(e)). At all temperatures, island formation takes place on the terrace *and* at preexisting iridium step edges.

Figures 1(a)–(e) show a marked decrease of the density of the graphene islands as the growth temperature is increased above 970 K. This decay corresponds to an increase of the island typical size, from a couple of nanometers to several tens of nanometers. Figure 1(f) shows the dependence of island density n on temperature, which displays a pronounced decrease of island density above 970 K.

It is visible in figure 1 that the island shapes depend on the TPG temperature. While at low TPG temperatures (figures 1(a) and (b)), only compact islands are visible, at 1120 K (figure 1(c)) smaller compact islands together with larger noncompact islands are visible. At higher temperatures (figures 1(d) and (e)), the islands are again compact. Note that at these temperatures nearly all islands are attached to the step and barely any islands are left on the terraces. Close-up images of typical islands zoomed to a comparable printing size show that the shapes are indeed different (figure 2). The very small islands formed at 870 K appear as spherical knobs with no specific features (figure 2(a)). After TPG at 970 K (figure 2(b)), these islands are compact with straight step edges oriented along the dense packed $\langle 10\bar{1}\rangle_{\mathrm{Ir}}$ directions of the substrate. On a local scale, the edges are always modulated with the periodicity of the moiré. At intermediate temperatures of 1120 K (figure 2(c)), the island edges are still along $\langle 10\bar{1}\rangle_{\mathrm{Ir}}$ directions, but the islands are no longer compact. A more compact shape is again observed at high temperatures of 1320 and 1470 K (figures 2(d) and (e)).

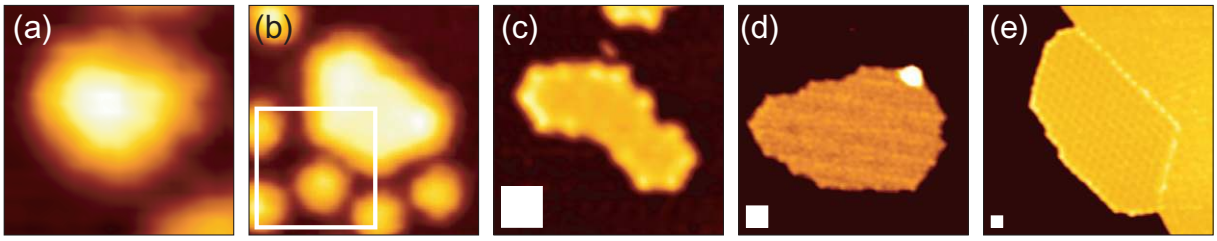

Figure 2. STM topographs of typical graphene islands prepared with the TPG procedure, after annealing for 20 s to (a) 870 K, 3.2 nm × 3.2 nm, (b) 970 K, 6.2 × 6.2 nm, (c) 1120 K, 18 nm × 18 nm, (d) 1320 K, 32 nm × 32 nm and (e) 1470 K, 64 nm × 64 nm. The size of the white box corresponds to the size of the smallest topograph (3.2 nm × 3.2 nm). The islands undergo a transition from an undefined, probably amorphous state over a compact shape at low temperature to noncompact shapes at intermediate temperature and (c) back to more compact shapes at high temperature.

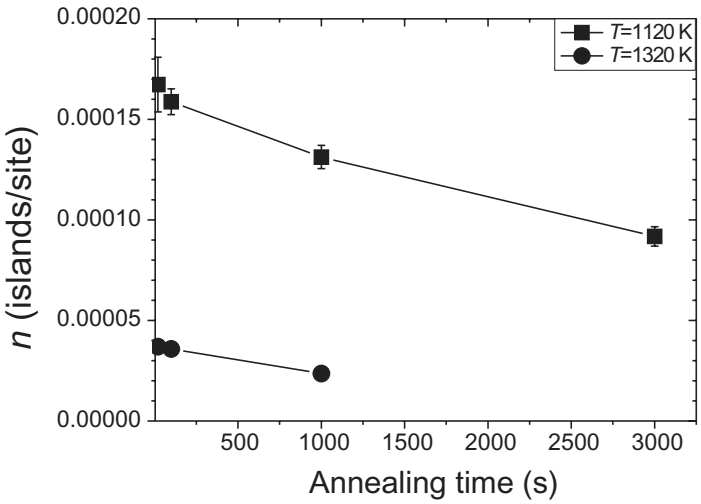

Figure 3. Density of graphene islands n as a function of the annealing time after annealing at 1120 K (squares) and 1320 K (filled circles).

The preferred edge orientation of the islands is parallel to the moiré high-symmetry direction and parallel to the $\langle 10\bar{1}\rangle_{\mathrm{Ir}}$ directions of Ir(111). As the $\langle 10\bar{1}\rangle_{\mathrm{Ir}}$ directions and the $\langle 11\bar{2}0\rangle_{\mathrm{C}}$ directions of graphene are aligned [28], the islands display $\langle 11\bar{2}0\rangle_{\mathrm{C}}$-oriented zigzag edges. The edges of epitaxial graphene will be discussed in detail in a forthcoming publication.

Figure 3 shows the evolution of the density of islands as a function of the annealing time at 1120 and 1320 K. Within 1000 s annealing, the island density has decayed by 25% at 1120 K and 35% at 1320 K, whereas the total graphene coverage is unchanged. These changes are only moderate compared with the changes in island density by increasing temperature (figure 1(e)).

The first step toward graphene formation is the thermal decomposition of ethene, which is complete at approximately 800 K [34]. The clusters obtained after TPG for 20 s at 870 K (figure 4(a)) possess a variety of heights and can therefore not be considered as graphene, which has a constant apparent height for each set of tunneling parameters. Forming carbon clusters by

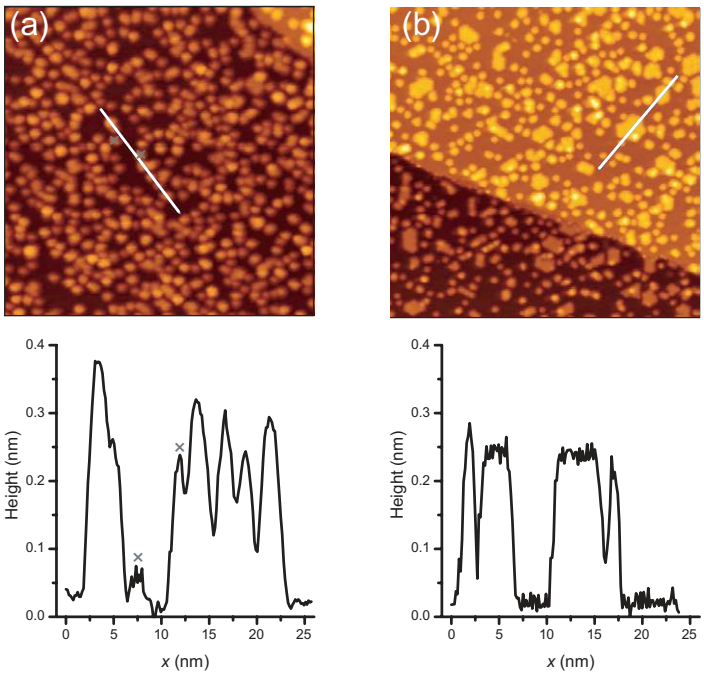

Figure 4. STM topographs (60 nm × 60 nm) of carbon islands prepared with TPG at (a) 870 K and (b) 970 K with corresponding height profiles. The height profiles show that in the case of the lower annealing temperature, the apparent height of the islands varies, whereas for an annealing temperature of 970 K the apparent height corresponds to the value of 0.21 nm as expected for graphene on Ir(111). (The peaks marked with an x must be disregarded, because there the profile is only crossing the periphery of the cluster.)

TPG at a temperature of 970 K yields flakes of homogeneous apparent height (figure 4(b)). These flakes show step edges along the dense-packed Ir(111) directions, just as graphene flakes grown at higher temperature do, indicating that the formation of graphene takes place at a temperature between 870 and 970 K. This situation is similar to TPG with ethene on Pt(111), where a transition from carbidic clusters to graphene takes place around 800 K [35].

In order to assess the amount of deposited molecules that was transformed into graphene, we exposed the Ir(111) surface for 30 s to an ethene flux in front of the gas doser resulting in a chamber pressure of 2×10^{-7} mbar. This exposure is even enough to ensure saturation coverage from the ethene background pressure only, regardless of the local pressure enhancement by the gas doser. The resulting coverage after TPG with an annealing time of 20 s results in an areal coverage of $(22 \pm 2)\%$ regardless of the temperature in the range 1120–1470 K. The graphene coverage θ corresponds to an initial ethene molecule density of $\nu_{C_2H_4} = \frac{1}{2}\theta\nu_C = 0.423 \times 10^{19}\,\mathrm{m}^{-2} = 0.27 \times \nu_{Ir(111)}$ and ν_{Ir} being the density of Ir(111) surface atoms of $1.57 \times 10^{19}\,\mathrm{m}^{-2}$. This is consistent with a weakly ordered $\sqrt{3} \times \sqrt{3}$ superstructure with less than $\frac{1}{3}$ ethene molecules per site and no loss of carbon during dehydrogenation [34]. The areal coverage with graphene for pressures below saturation was used as a calibration mark for the characterization of the gas dosing tube as described in section 2.

To demonstrate the versatility of the TPG method coronene ($C_{24}H_{12}$) molecules were also employed to grow graphene. An areal coverage of $(130 \pm 10)\%$ was deposited at 125 K

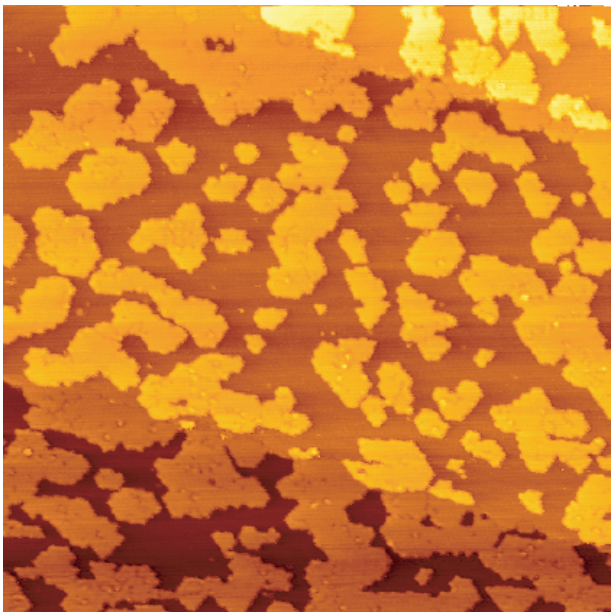

Figure 5. STM topograph (125 nm × 125 nm, imaged at 300 K) of graphene prepared by TPG at 1120 K. 1.3 ML of coronene adsorbed at 125 K was used as a molecular starting layer.

and imaged with STM. TPG at 1120 K for 20 s results in the formation of graphene islands (figure 5), with a $(55 \pm 3)\%$ areal coverage. This coverage corresponds to an areal density of $\nu_{C_{24}H_{12}} = (8.8 \pm 0.5) \times 10^{17}\,\mathrm{m}^{-1} = (0.056 \pm 0.003) \times \nu_{Ir(111)}$. The amount of carbon in the graphene after heating is less than the amount that has been deposited in the form of coronene. However, the coverage corresponds to the carbon from a saturated monolayer of coronene on a metal (e.g. on gold: molecule density of $(8.7 \pm 1.6) \times 10^{17}\,\mathrm{m}^{-1}$) [36]), which is close to a densely packed flat layer of coronene molecules as estimated from the van der Waals radius ($10 \times 10^{-17}\,\mathrm{m}^{-1}$). This indicates that only the first layer takes part in the decomposition process, while additional molecules are desorbed during the sample heating. The higher degree of coverage from TPG with coronene in comparison to ethene is easily understood as the saturated coronene layer bears more carbon atoms in a given area than the saturated ethene layer.

3.2. Discussion

3.2.1. Edges and substrate interaction. The global orientation of the graphene edges as well as atomically resolved images show that in the system studied here edges are predominantly of the zigzag type. The edges are most probably terminated by unsaturated carbon atoms as found in the related system graphene/Pt(111) [37]. The preference for zigzag edges can be understood in terms of unsaturated carbon bonds as the zigzag edge has a factor of $\sqrt{3}$ less of these twofold coordinated C atoms with respect to an armchair edge, and is therefore energetically favored. The prevalence of zigzag edges is in contrast to the situation found for hydrogen-terminated extended graphene-like molecules (polycyclic aromatic hydrocarbons), where the armchair edge is kinetically more stable [38].

The occurrence of straight steps in graphene islands is a sign of a thermally activated process allowing carbon atoms to move at the step. This process appears to be rather slow, as larger islands are not in their equilibrium shape. The simplest process to enable transport of atoms along the step edge is the jumping of single C atoms bound to the step in a phenyl-like geometry from one binding site to the next. However, as already a C–C single bond is rather strong ($\approx$4 eV) this process only becomes activated (i.e. happens with a frequency of 1 Hz) at $\approx$1500 K (using as an attempt frequency the respective stretching mode of toluene [39]). Therefore, more complex cooperative processes must take place here. Examples for such mechanisms are known for small polycyclic aromatic hydrocarbons, where it was shown that step adatoms in the form of heptagons inside the chain of hexagons or advacancies in the form of pentagons can efficiently diffuse already at lower temperatures [40, 41]. C diffusion at the edges could proceed through the prominent role of C pentagons continuously formed at graphene edges, further migrating then colliding, eventually resulting in the formation of the C hexagon building blocks of graphene [42]. Such processes have strong similarities with those describing soot formation initiated by H atoms [43]. The presence of H atoms in the present system is unlikely but the initiation of the reaction could also be mediated by Ir.

Graphene islands at iridium step edges grind into the preexisting step edge, deforming it significantly. The one-dimensional (1D) interface between the Ir step and the graphene flake is always straight apart from the periodic small-scale modulation with moiré periodicity mentioned above. The step straightening of the Ir–C step interface is very efficient. Edge diffusion may be facilitated by the diffusion of Ir along the edge, which is present at the temperatures used for graphene growth [44].

3.2.2. Ripening. In order to understand the reduction of island density with increasing annealing temperature, we have to consider a process which can transform a morphology as depicted in figure 1(b) into the morphologies of (c)–(e).

All annealing experiments start from the same initial state. This implies that the result of a TPG cycle with 1470 K will have had the lower temperature results of TPG as intermediate states.

Two ripening mechanisms are candidates for such a process: first, Ostwald ripening, i.e. the preferential growth of large islands at the expense of dissolution of small ones through their higher 2D vapor pressure of carbon adatoms (or small clusters thereof) [45]. Second, Smoluchowski ripening, i.e. the reduction of island density through mobile islands coalescing upon contact [46].

Ostwald ripening implies the evaporation of carbon atoms from the graphene islands. As considered above, the detachment of carbon atoms from the edge is unlikely for temperatures below 1500 K. At a temperature of 1120 K where ripening takes place, the resulting detachment frequency of 1×10^{-5} Hz is too low to contribute significantly to the coarsening at a timescale of seconds.

With Smoluchowski ripening entire islands move. At first glance, it may seem counterintuitive that nanometer-sized islands move, regarding the large number of carbon atoms binding to the iridium substrate. However, it becomes plausible considering that graphene is incommensurate on Ir(111). As the island is very rigid, the graphene structure does not lock into the periodicity of the substrate at a specific registry. This implies that the barrier for movement is negligible, because for every carbon atom that is moved away from its optimum-binding site, another atom gains energy by slipping towards a good binding site. Probably only the atoms

at the edge are more strongly bound to the substrate and possibly without a counterpart in the lattice to compensate for the displacement may eventually experience a barrier for island diffusion. The activation energy should roughly scale with the perimeter of the island.

Our data are strongly in favor of Smoluchowski ripening, i.e. of graphene island diffusion and coalescence. Assuming Smoluchowski ripening, our island shape observations can be interpreted as follows. The observed island density decrease is through continuous island diffusion and coalescence. Specifically with the completion of the transition from carbidic clusters to graphene islands, a strong increase of island mobility takes place explaining the dramatic decrease of island density above 970 K. If at 1120 K small compact graphene islands with dense packed step edges touch during island diffusion, they coalesce. However, as the time needed to reshape an island to its compact, minimum energy shape is a strongly increasing function of island size (it increases by the power 3–4 with the diameter of the final compact island [47]) coalesced islands are not able to reshape on the timescale of the TPG experiment (incomplete coalescence). Therefore, as observed, large, irregularly shaped islands resulting from fresh incomplete coalescence together with small compact islands are present after TPG at 1120 K (cf figures 1(c), 2(c) and 5). In particular, the presence of inclusions in large irregular islands as visible in the inset of figure 1(c) becomes understandable as the result of incomplete coalescence of several islands. After TPG at higher temperatures, the mobile graphene islands are found to be nearly completely at steps (figures 1(d) and (e)). During their random walk the mobile islands hit steps, where they get stuck (see also below on the binding mechanisms). Once the graphene islands stick to steps, their mobility along the step is likely to be reduced compared with the mobility on terraces, coalescence becomes thus rare and the islands have again sufficient time to maintain a compact shape. Note that due to the sticking of graphene islands to steps no clear power law dependence of island number density on annealing time can be expected [48].

Assuming to the contrary Ostwald ripening through the attachment and detachment of single carbon adspecies, the appearance of irregular shaped large islands and inclusion in these is not understandable. Also the disappearance of all, even the largest islands, from terraces is hard to understand in the absence of graphene island mobility.

4. CVD

4.1. Results

Figure 6 shows a sequence of STM topographs of the Ir(111) surface after CVD growth of graphene was performed at 1120 K. The ethene dose was increased from figures 6(a)–(d), maintaining the ethene partial pressure at the ion gauge at 5×10^{-10} mbar and increasing the time the hot Ir(111) surface is exposed. Graphene is unambiguously identified by a well-defined height and the occurrence of a moiré superstructure [9, 27, 28]. The insets in figure 6(a)–(d) highlight the regions of the surface which are covered with graphene. We make the following observations: (i) graphene is exclusively located at the substrate step edges for low coverages, (ii) graphene frequently spans both sides of the step edge, (iii) the larger fraction of graphene is on the lower terrace (70% for doses of 4×10^{-8} mbar s) and (iv) while there are graphene flakes attached only to an ascending step edge, no graphene flakes were ever observed attached only to a descending step edge. At low doses, it is possible to make out the graphene location with respect to the step edges (ascending/descending); this is no longer possible at larger doses due to the coalescence of growing islands and the growth of islands over steps.

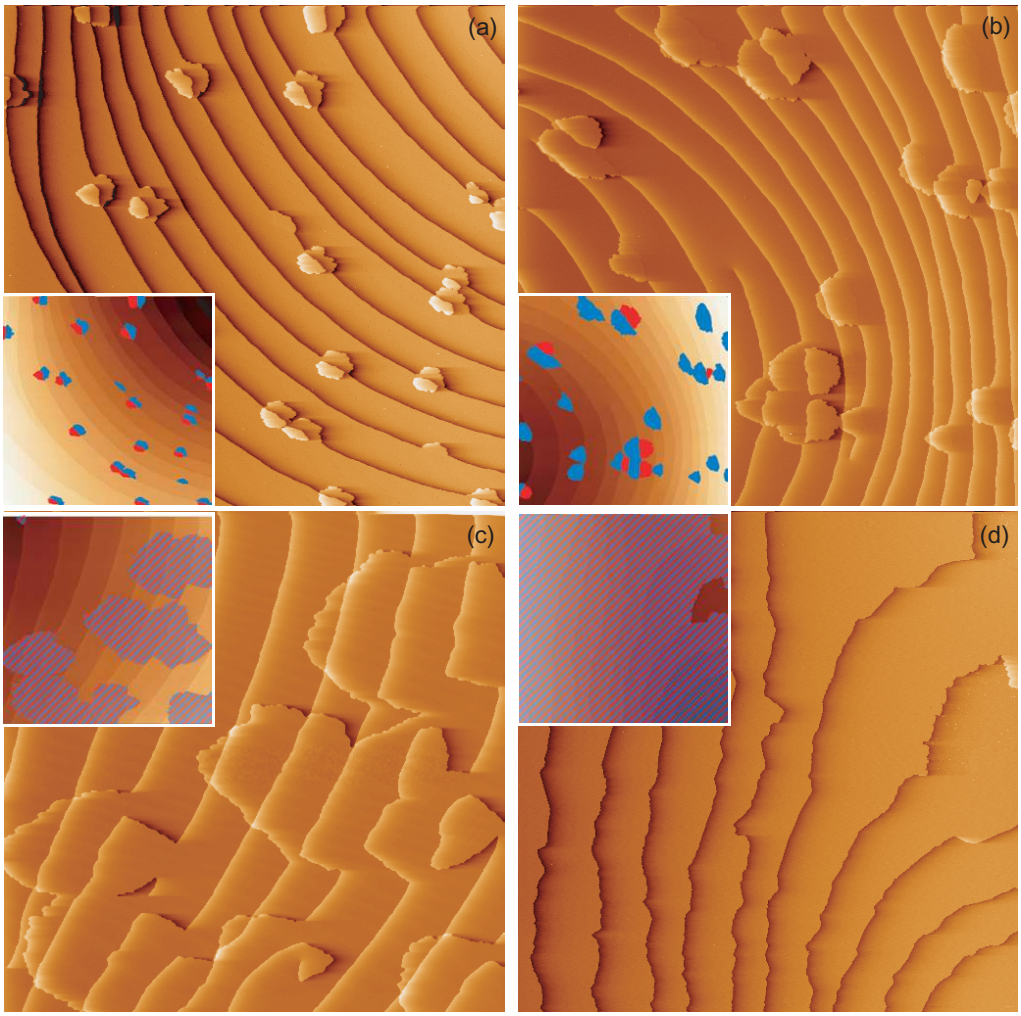

Figure 6. Differentiated STM topographs (1 μm $\times$ 1 μm) at 300 K of graphene grown on a Ir(111) surface at 1120 K, by exposure to an ethene partial pressure of 5×10^{-10} mbar, during 20 s (a), 40 s (b), 160 s (c) and 320 s (d). Insets are scaled down versions of the large topographs: (a, b) graphene on lower (upper) terraces is marked blue (red) and (c, d) graphene areas are colored blue/red.

At 1120 K, CVD enables full coverage of the Ir(111) surface. For a given ethene partial pressure, the graphene coverage as a function of the dose first linearly increases, and then asymptotically approaches 100% with a decreasing rate (figure 7(a)). The coverage increase is accompanied by a decrease of the island density, already after the lowest dose of 20 s ethene (5×10^{-10} mbar) employed (figure 7(b)). Therefore, coalescence is already in progress at the second lowest dose of 40 s ethene, i.e. for a coverage of 10%. The uniform size of graphene islands for the dose of 20 s of ethene suggests that the nucleation stage is already over whereas coalescence has not yet started. CVD growth was also performed with higher ethene pressures. For higher ethene pressures (4×10^{-9} mbar (diamond in figure 7) and 5×10^{-9} mbar (triangle in figure 7)), the coverage appears to be lower after the same ethene dose.

The crystallinity of graphene at various stages of the CVD procedure at 1120 K was investigated taking benefit of the moiré appearing in magnified STM topographs. Figure 8(a)

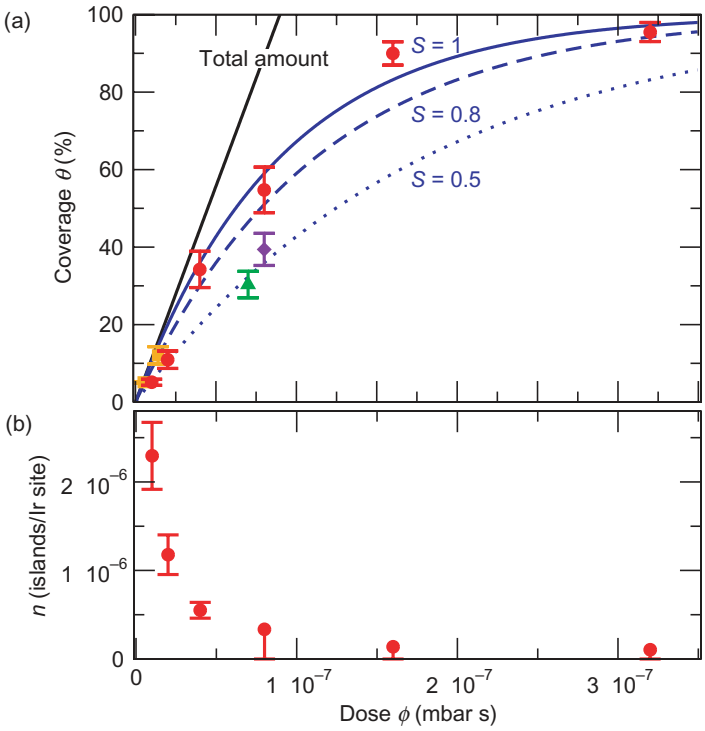

Figure 7. (a) Average graphene coverage θ over the Ir(111) surface, as a function of the ethene dose ϕ at 1120 K. Experimental data for a partial pressure of $p = 5 \times 10^{-10}$ mbar are shown as red circles. Orange squares, purple diamond and green triangle correspond to 1×10^{-9}, 4×10^{-9} and 5×10^{-9} mbar, respectively. The modified Langmuir adsorption model described in the text is shown for a sticking coefficient $S = 1$ (no desorption), $S = 0.8$ and $S = 0.5$ as solid, dashed and dotted blue lines, respectively. The dark solid straight line stands for the hypothetical coverage that would be achieved if all the provided ethene molecules participated in graphene growth, including those landing on the growing graphene islands. (b) Graphene island density n as a function of the ethene dose for a 5×10^{-10} mbar ethene partial pressure.

is typical of a graphene island extending on both sides of a substrate step edge. As highlighted in the inset of figure 8(a), there is a single moiré domain which spans across the step edge. This was recently shown to be indirect evidence for full structural coherency of graphene [9]. The Ir(111) step edge underneath is partly aligned with the high-symmetry direction of the moiré. This situation, which corresponds to a $\langle 10\bar{1}\rangle_{\mathrm{Ir}}$ iridium step edge parallel to a $\langle 11\bar{2}0\rangle_{\mathrm{C}}$ graphene direction, has evolved from profound reshaping occurring during graphene growth. This reshaping of the iridium step edge that was originally smooth (see the typical situation of figure 6) is highlighted by the black line in the inset of figure 8(a). In the case where substrate step edges are not aligned with the high-symmetry directions of the moiré pattern (lower part of graphene island in figure 8(a)) the moiré orientation is often not preserved across the step edge. Still, a continuous graphene lattice is ensured by the formation of edge dislocations, such as the two ones visible at atomic scale in figures 8(b) and (c). These dislocations appear as bright protrusions at nanometer scale [9]. One is indicated by the arrow labelled (2) pointing

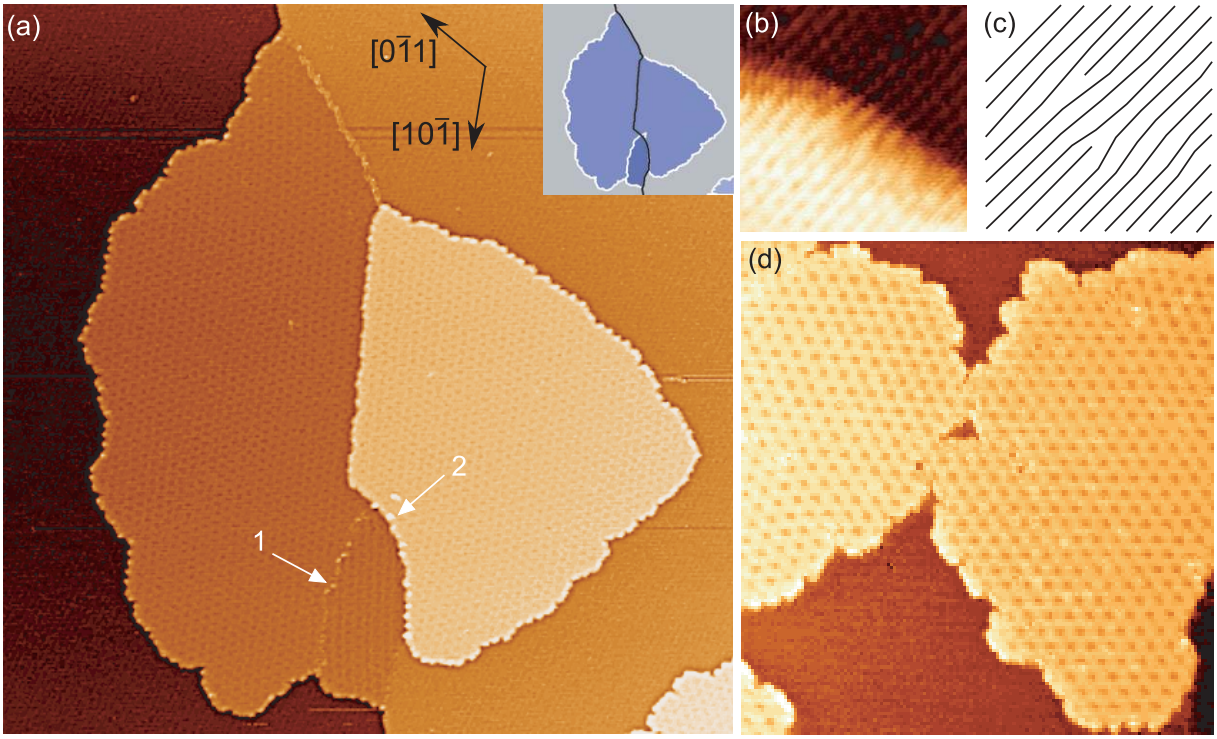

Figure 8. (a) STM topograph (171 nm × 171 nm) of graphene grown by CVD on a Ir(111) surface at 1120 K, out of exposure to an ethene partial pressure of 5×10^{-10} mbar, during 40 s. The arrows point out edge dislocations at the boundary between two moiré domains, at a terrace (1) and in close vicinity of the step edge (2). The black arrows show the orientation of the Ir(111) substrate throughout this figure. The inset shows the Ir(111) surface (gray) supporting graphene and exhibiting a step edge (black line). Different orientations of the moiré are visualized with blue tones. (b) STM topograph (2.7 nm × 2.7 nm) of graphene across a substrate step edge, and (c) a corresponding line network of C rows showing two edge dislocations. (d) STM topograph (70 nm × 73 nm) of two coalesced islands forming a coherent graphene island (exposure to 5×10^{-10} mbar ethene for 20 s).

to the step edge in figure 8(a); it is similar to the one designated by the arrow labelled (1) in figure 8(a) or to those visible in figure 9. As a whole, graphene flakes after CVD at 1120 K include moiré domains with typical extension between several tens of nanometers and a couple of hundred nanometers, some extending across step edges, and structurally coherent through edge dislocations.

Upon coalescence, growing graphene islands become coherent. This is pointed out in figure 8(d), where one observes the continuity of the moiré between two islands, though the orientation of the moiré differs from one island to the other. This implies that the atomic graphene lattices of the two islands match upon coalescence. The slight misorientation of the islands amplified by the moiré is accommodated by edge dislocations [9].

Annealing has a noticeable effect upon the structural quality of graphene grown by CVD. Firstly, the irregular graphene edges observed after growth at 1120 K (figure 9(a)) are smoothed by an annealing step at 1220 K for several tens of seconds (figure 9(b)). Secondly, dark dots,

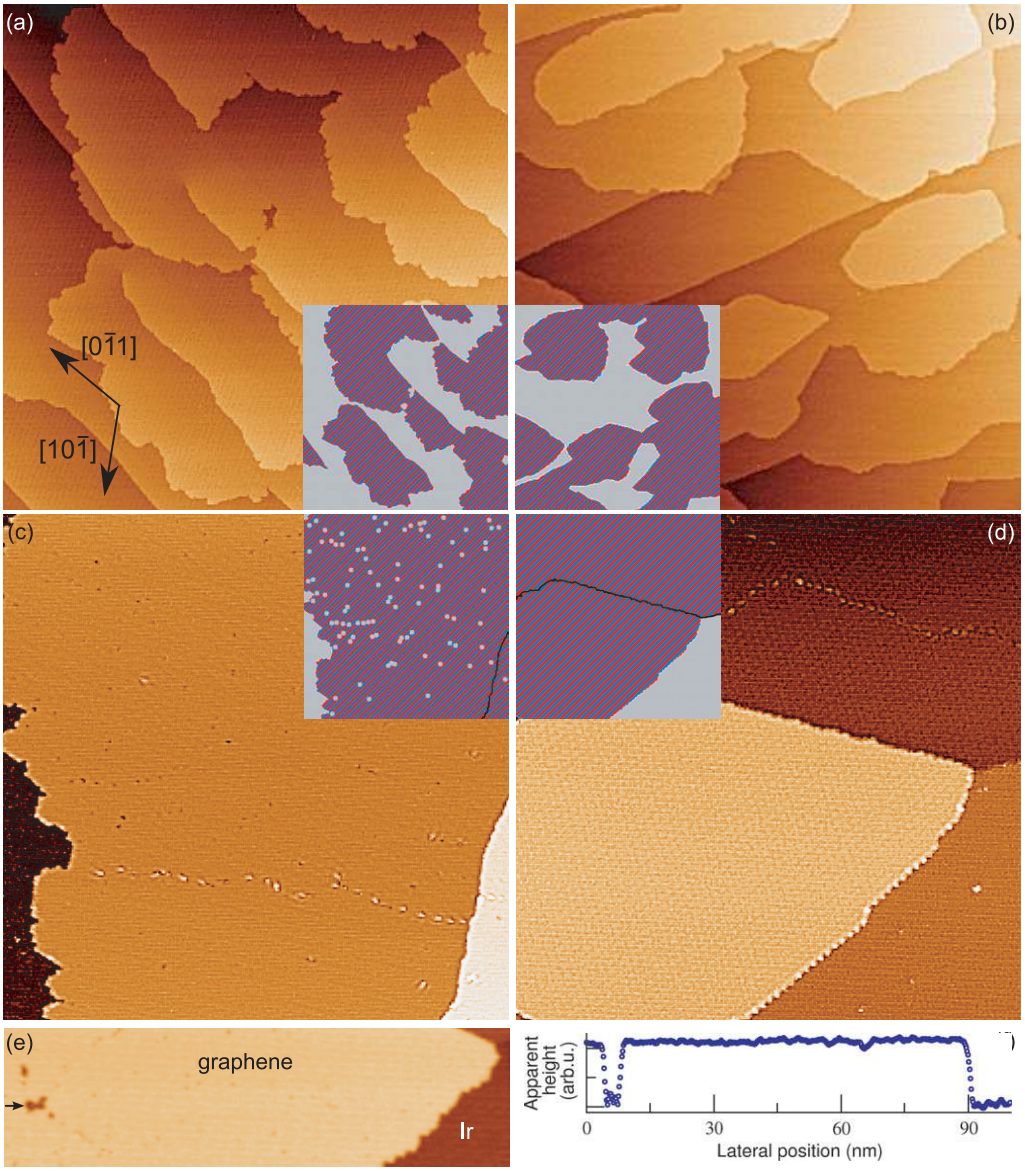

Figure 9. STM topograph of graphene grown by CVD on a Ir(111) surface at 1120 K, with an ethene partial pressure of 5×10^{-10} mbar, during 80 s, before (a, c) and after (b, d) annealing for 40 s to 1220 K. Image size is 500 nm × 500 nm for (a, b) and 125 nm × 125 nm for (c, d). Insets show the graphene (hashed areas) on top of Ir(111) (gray). Inset of (c) highlights holes (gray spots) in graphene, insets of (c) and (d) highlight the Ir step edge (black line). (e) STM topograph (102 nm × 28 nm) of graphene grown by CVD on a Ir(111) surface at 1120 K, after exposure to an ethene partial pressure of 4×10^{-9} mbar for 20 s, and (f) apparent height profile along the horizontal passing through the arrow in (e).

with sizes ranging from a fraction of a nanometer to a couple of nanometers, are observed in graphene as prepared through CVD. These features systematically appear as depressions in the graphene layer. Some of them, like the one near the arrow in figure 9(e), are large enough for

sharp STM tips to image the Ir(111) at the bottom. This is apparent in the height profile passing through this hole (figure 9(f)). We then conclude that they are holes in the graphene layers that could have been trapped during growth. While the smallest features may consist of C vacancies or divacancies [49], some of the largest ones could have evolved from the agglomeration of small vacancies [50, 51]. The density of these holes in graphene as prepared through CVD at 1120 K with 5×10^{-10} mbar ethene during 80 s (figure 9(c)), is reduced upon a 1220 K annealing step, from several 10^{-5} per Ir site to at least two orders of magnitude less (figure 9(d)). It also decreases as the exposure time to ethene during CVD at 1120 K is increased. For instance, after 640 s with 5×10^{-10} mbar ethene, the density has decreased by almost one order of magnitude with respect to the situation after 80 s.

Increasing the CVD growth temperature results in graphene with improved structural quality, i.e. a better defined orientation and lower density of edge dislocations [9]. At 1320 K, single orientation is preserved across μm distances and substrate step edges, with no edge dislocation. Already for the lowest ethene doses employed (2×10^{-8} mbar s), CVD at 1320 K yields graphene flakes with at least μm extensions separated by at least μm distances. Figure 10(a) shows part of a graphene island (upper right corner) sitting on a large, bare iridium region. Coverage increases with ethene dose, either because the size or the density of graphene islands increases. In fact, addressing the issue of graphene/Ir(111) morphology achieved by CVD at 1320 K is made difficult by the μm field of view limitation of our STM.

Decreasing the growth temperature has no noticeable effect on the overall graphene coverage (figure 11), consistent with the results of TPG and the absence of desorption. It induces a marked decay of the typical size of graphene islands (figure 10). Being in the μm range for 1320 K growth temperatures this quantity is one, two and three orders of magnitude smaller for 1120, 970 and 870 K, respectively. This decrease is accompanied by an increase of the density of islands at the substrate step edges, in such a way that the steps are almost fully covered with graphene at 870 K.

At moderate growth temperature (870 and 970 K), STM topographs show that the graphene coverage at the substrate step edges is a well-defined quantity for a given ethene dose. It does not seem to depend on the terrace width (from less than 10 nm to several hundreds of nanometers), as seen in figure 12(a). Whether this is also the case at higher temperatures (1120 or 1320 K) could not be determined due to the limited field of view of the STM.

Whatever the growth temperature, substrate step edges play a prominent role. There graphene nucleates from 970 K on. At 870 K, nucleation is still highly preferential at the step edges, but graphene occasionally forms at the substrate terrace, as observed in figure 12(b).

4.2. Discussion

4.2.1. Graphene nucleation. As just shown (figure 12(b)), at 870 K graphene not only nucleates at the substrate step edges, but also rarely on the terraces. Consistent with our results for TPG, we interpret this observation as due to the thermal decomposition of ethylene everywhere on the sample surface, i.e. at steps and on the terraces. Above 870 K, graphene islands are only found at step edges, meaning that the C adspecies resulting from catalytic thermal decomposition of ethene is highly mobile. The decrease of the 1D graphene island density with temperature, i.e. the increase of island separation along the step with temperature, is evidence that nucleation along the step is homogeneous and not at specific defect sites. We frequently observed graphene islands extending from the step only onto the lower terrace, but

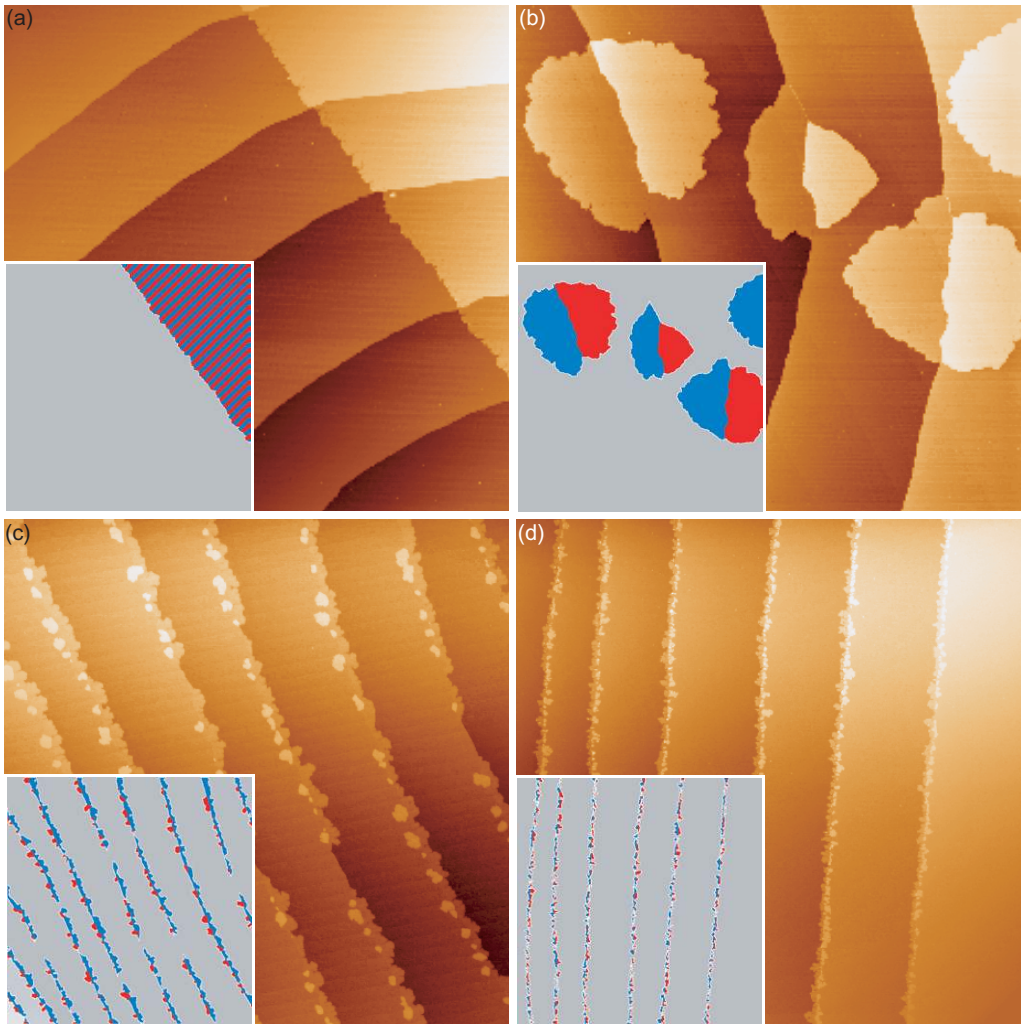

Figure 10. STM topograph (455 nm × 455 nm) of graphene grown by CVD on a Ir(111) surface at 1320 K (a), 1120 K (b), 970 K (c) and 870 K (d). The ethene partial pressure used for the growth of graphene is 5×10^{-10} mbar, and the exposure time is 40 s, except for (a) where it is 80 s. Insets show graphene as hashed areas or in red (blue) when attached at a descending (ascending) step edge.

never islands extending from the step only onto the upper terrace. As the areal fraction of islands is also larger on the lower terrace (observation (iii)), we assume that nucleation at the step takes place only at the lower terrace. The enhanced nucleation probability adjacent to the step on the lower terrace may be due to a larger C adspecies concentration or due to a smaller size of the critical nucleus (a smaller nucleation barrier). While for graphene on Ni(111) a higher adspecies concentration was predicted [52, 53], we speculate that for Ir the size of the nucleation barrier is lower. We noticed already for TPG and CVD that the edges of graphene islands intensely interact with Ir steps. The most plausible reason is the formation of partial bonds between graphene edge atoms and step atoms of σ character. The formation of such bonds reduces the total edge energy of a graphene nucleus, which reduces the height of the nucleation barrier. Whether C adspecies

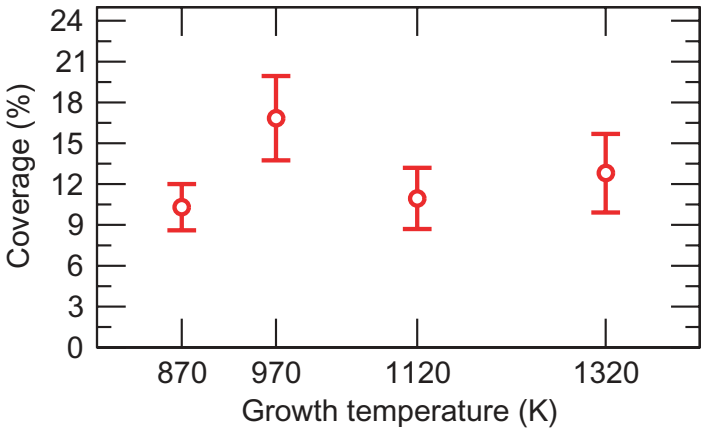

Figure 11. Graphene coverage as a function of the CVD growth temperature, for an ethene dose of 2×10^{-8} mbar s.

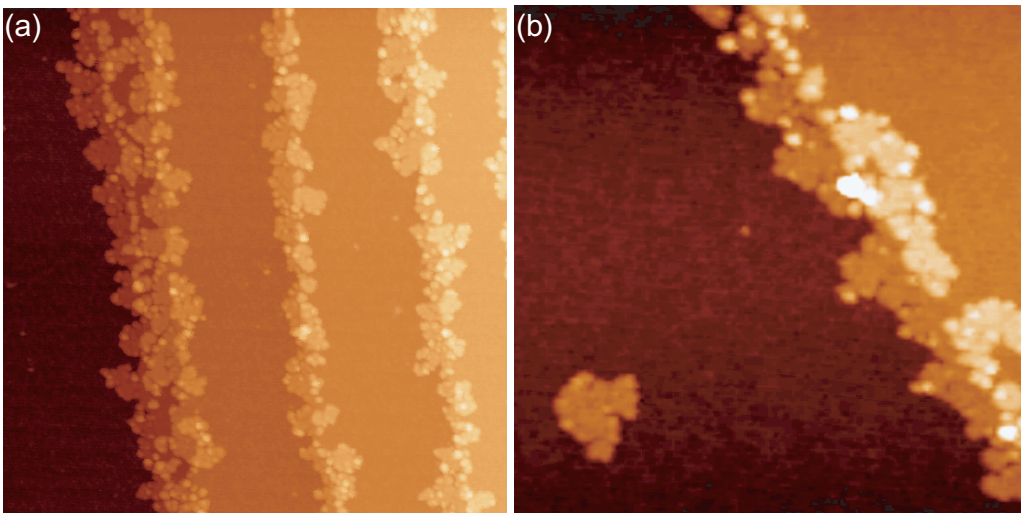

Figure 12. STM topographs of graphene grown by CVD at 870 K with a dose of 2×10^{-8} mbar s. (a) 110 nm × 110 nm and (b) 70 nm × 70 nm.

already bind to Ir step atoms is an open question. If yes, a concentration increase of the adspecies at the step would result, giving rise to a further enhanced nucleation probability. As depicted in figures 13(a) and (b), a maximum number of C–Ir bonds can be formed if Ir step edges align to graphene's more stable zigzag edges, i.e. if the $\langle 10\bar{1}\rangle_{\mathrm{Ir}}$ direction is parallel to the $\langle 11\bar{2}0\rangle_{\mathrm{C}}$ direction, which also corresponds to a high-symmetry moiré direction (figure 8(a)).

We therefore propose the following scenario for nucleation of graphene islands as typical: the C adspecies (figure 13(a)) nucleate at the lower side of a step edge in the energetically most favorable configuration, i.e. with $\langle 10\bar{1}\rangle$ Ir steps aligned with $\langle 11\bar{2}0\rangle$ graphene steps. In order to maximize the contact of the two steps (figure 13(b)), the graphene island will reshape the Ir step during growth.

Growth at the upper part of step edges can only take place in the presence of graphene at the lower terrace, namely if C atoms can form σ bonds with the C atoms at the terrace below.

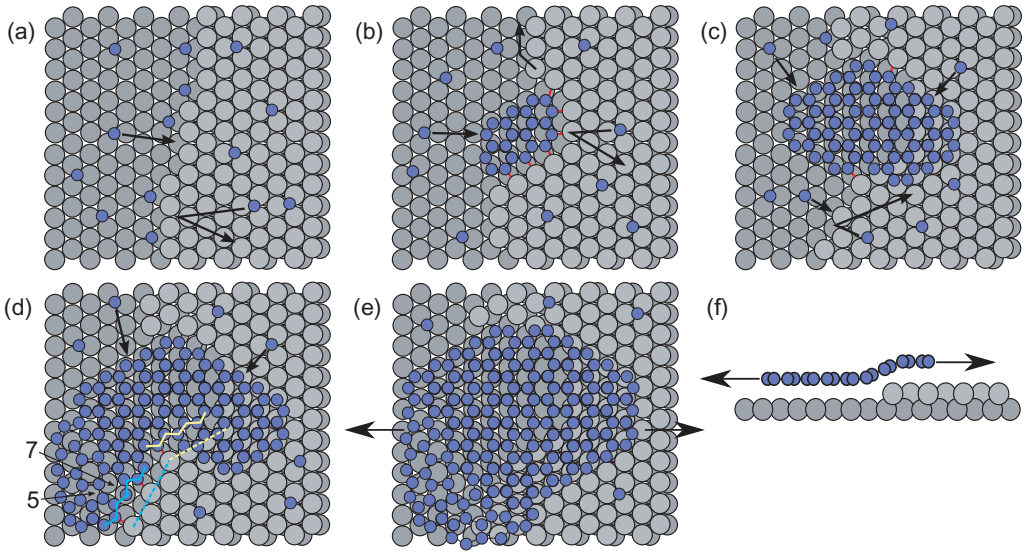

Figure 13. Top-view (a–e) and side-view (f) ball models of the growth of graphene on Ir(111). Carbon and iridium atoms are shown as purple and gray circles, respectively. Arrows schematically indicate either some of the atom movements (a–e) or graphene growth rate (f). C–Ir bonds at the step edge are shown as red lines. Zigzag carbon edges of two misoriented domains are highlighted in (d) as thick solid lines; the undistorted zigzag edge lies parallel to the iridium $\langle 10\bar{1}\rangle$ step edge highlighted as dotted lines (yellow). A heptagon–pentagon (7 and 5 labels in (d)) pair is present at the boundary between the two domains (d, e) and allows one domain to tilt.

This implies crossing the energy barrier for breaking the C–Ir bond first, which may require numerous attempts. The growth at the upper terrace would then be delayed (figure 13(c)). This accounts for the observed relative areal proportion of graphene at ascending/descending step edges of 7/3. The single orientation of graphene on both sides of a straight step edge (figure 8(a)) underlines the full structural coherency of the graphene lattice, which lies on the step like a blanket [9]. The energy cost of graphene covering a step edge is lower, the lower the associated plastic or elastic deformation of the graphene lattice. Therefore growth at the upper terraces first takes place across a dense substrate step along a $\langle 10\bar{1}\rangle_{\mathrm{Ir}}$ direction, as shown in figure 13(c) and observed on STM topographs like figure 8(a). This might also be an additional driving force for reshaping substrate step edges. We speculate that once a graphene island has overgrown a step edge, reshaping of the Ir step ceases. Further growth of the graphene island on the lower terrace then has to match a less favorable step orientation. This will generally imply a tilt of the graphene atomic rows and cause the formation of a tilt boundary between island parts matching differently oriented Ir substrate steps (figure 13(d)).

Growth over steps is observed neither for graphene on Ru(0001) [19] nor for carbon nanotubes on Ni nanoparticles [54]. In these two cases, growth only proceeds from the ascending step edge. In particular, the distance between the carbon plane and a Ru(0001) surface (0.145 nm [19]) is smaller than the substrate step height (0.220 nm). This is in agreement with the deep modification of the electronic structure of the first graphene layer on Ru(0001) [19, 32, 33], or of graphene on Ni(111) [16, 17], which suggests hybridization between graphene

π-bands and metal bands, i.e. the formation of chemical C–metal bonds. In this respect, the case of graphene on Ir(111) is very different. Indeed, the distance between the graphene plane and the Ir(111) surface was predicted to be 0.34 nm, on the basis of density functional theory (DFT) calculations [55]. This is close to the distance between graphene planes in graphite (0.334 nm), and is consistent with recent results showing the weak electronic interaction with the Ir substrate [15]. The graphene height provided by DFT (0.34 nm), is larger than the Ir(111) step height (0.22 nm), which probably makes the σ-like C–Ir bonds at the step edges much less stable than in the case of Ru or Ni step edges, and allows graphene to grow over steps (figures 13(d) and (e)).

4.2.2. From islands to full coverage. The size of graphene islands increases first through growth over ascending and descending step edges by incorporation of mobile C adspecies or small clusters resulting from dehydrogenation of ethene, and second through coherent coalescence of graphene islands.

More can be learnt about graphene CVD growth by analyzing the surface coverage θ as a function of ethene dose ϕ. We assume a modified Langmuir adsorption model: ethene molecules stick to identical and independent unoccupied Ir sites with probability S, and are removed instantaneously from these sites to form graphene islands covering a fraction θ of the Ir surface. Ethene molecules arriving on graphene islands either do not stick to them or desorb immediately, unable to reach the sticky Ir substrate. Carbon diffusion into the bulk in iridium is known to be much less than in other transition metals like Ru, Rh or Re [56], and is therefore neglected in the following. Whatever the value of S, θ is lower than expected if all impinging ethene molecules were transformed into graphene (solid black curve in figure 7(a)). Our model assuming adsorption of ethene to Ir only yields

$$\theta = 1 - \mathrm{e}^{-\phi \times S \times \Omega / \sqrt{2\pi M k_\mathrm{B} T}}, \tag{1}$$

where M is ethene molar mass, k_B the Boltzmann constant, T the temperature of the gas molecules and $\Omega = 5.2 \times 10^{-20}\,\mathrm{m}^2$ the unit area for C in graphene on Ir(111). As seen in figure 7(a), this simple model with $S = 1$, i.e. 0% ethene desorption from Ir and no diffusion into the bulk, fits quite well the measured coverages for an ethene partial pressure of 5×10^{-10} mbar (circle symbols), without any adjustable parameter. This is a strong indication for no desorption, as also pointed out by the roughly constant graphene coverage as a function of growth temperature, shown in figure 11. As the assumption $S = 0.8$ leads only to a slightly worse agreement with the data, we note that our conclusion has to be taken with caution.

At lower growth temperatures, 870 and 970 K, STM shows that the graphene growth rate at the step edges is independent of the substrate terrace—catalytic—area (figure 12(a)). This markedly differs from the situation of graphene on Ni(111), where the step coverage was claimed to scale with the terrace size [57]. The behavior we observe is an indication for an interface-limited growth, namely C incorporation at the graphene edges is the limiting step. For interface-limited growth, no concentration gradients of the adspecies are developed. Contrary to diffusion-limited growth, the presence of a graphene island then would not decrease the nucleation probability of another island in its vicinity. The early coalescence of graphene islands, which is already in progress for coverages as low as 10% (figures 6(a) and 7(b)) supports this view. Indeed, onset of coalescence for such a low coverage is well reproduced assuming random nucleation of graphene at step edges and a uniform C adspecies concentration over the Ir(111) surface. Finally, the influence of the pressure upon coverage could also be interpreted in

terms of interface-limited growth. In particular, increasing the pressure to 4–5 $\times 10^{-9}$ mbar, i.e. by a factor of 10 (7×10^{-8} and 8×10^{-8} mbar s doses, corresponding to triangle and diamond symbols in figure 7(a)), yields coverages that are not accounted for by $S = 1$. This could be an indication for C desorption during the limiting step.

During the time C incorporation at graphene edges takes, C adspecies not directly in contact with graphene could either desorb, diffuse into the bulk, or travel μm distances until they encounter graphene islands where they could incorporate (surface diffusion from high to low density of steps regions). For an ethene partial pressure of 5×10^{-10} mbar, however, desorption is ruled out at 1120 K, as shown before. Therefore at lower temperature and the same pressure, it should also be irrelevant. Even if it is relevant at 1120 K but a higher ethene partial pressure (4–5 $\times 10^{-9}$ mbar) as argued previously, assessing the activation energy for desorption at 1120 K yields a frequency of 1×10^{-4} Hz at 870 K, which is negligible. Therefore, surface diffusion over large distances is the prominent process already at 870 and 970 K. This might account for the large typical length scales in the graphene/Ir(111) morphologies achieved at 1120 K, and to a larger extent at 1320 K.

4.2.3. Carbon mobility in and at the edges of graphene. Finally, the compact morphology of the graphene islands is evidence for efficient C diffusion at the graphene edges. This was discussed earlier as accounting for the straight edges observed for the graphene islands grown through TPG. Annealing effects, namely smoothening of graphene edges and quenching of vacancy (hole) density, provide strong evidence for C or vacancy mobility to and at the step edges. Vacancy defects in graphene and heptagon–pentagon pairs, the latter were recently claimed to evolve from the former in C nanotubes [51], are both expected to be mobile if the corresponding energy barrier is low enough. It was predicted that C vacancy diffusion in graphene has a $\sim$1 eV energy barrier [49], corresponding to 10^{-2} Hz phenomena at room temperature, and consistent with real-time observations in carbon nanotubes, for vacancies or divacancies [58, 59] and even much larger vacancies [50]. Heptagon–pentagon pairs were also observed to be mobile [59]. At the temperature of interest here, vacancy or defect diffusion should be significant, and so should diffusion through the island interior to the edges. Notably, these C transport processes via the interior of the islands could also be involved in the smoothening of the edges of graphene islands grown by TPG.

5. Conclusion

We have investigated two complementary approaches for graphene on metal preparation, namely TPG and CVD. Both lead to graphene characterized by a moiré superstructure with a preferential orientation favored at high growth temperatures, and by a well-defined height, corresponding to a single layer. Growth proceeds in the presence of the bare catalytic Ir surface, which catalyzes the decomposition of the C-containing molecules (ethene or coronene here); therefore, the growth is self-limited to precisely one layer of graphene. Whatever the method, the substrate step edges are reshaped by the growing graphene, and C or vacancy diffusion is involved at the graphene edges.

The two approaches result in distinct morphologies. TPG gives graphene nanoislands with controllable size, from a couple of nanometers to several hundreds of nanometers depending on the growth temperature, with well-defined zigzag edges and shapes close to equilibrium. The islands exhibit Smoluchowski ripening above 970 K. CVD allows to tune the graphene

coverage up to 100% of the sample surface, with a very high structural quality above 1120 K. Graphene weakly interacts with iridium, and crosses step edges while maintaining its structural coherency. Still, substrate step edges, especially ascending ones, play a decisive role for graphene nucleation. There is an indication that the limiting step of graphene CVD growth is incorporation of the carbon adspecies at the graphene edges.

Graphene nanoislands grown by TPG are promising candidates for the investigation of the specific electronic properties of zigzag edges, and regarding quantum confinement of the Dirac-like charge carriers in graphene. CVD provides a reproducible method for the controlled preparation of macroscopic single-layer graphene with high crystalline quality.

Acknowledgments

JC thanks the Alexander von Humboldt foundation for a research fellowship. Financial support through the DFG research grant 'Two dimensional cluster lattices on graphene moirés on dense-packed metal surfaces' is acknowledged.

References

[1] Novoselov K S, Geim A K, Morozov S V, Zhang Y, Dubonos S V, Grigorieva I V and Firsov A A 2004 Electric field effect in atomically thin carbon films *Science* **306** 666

[2] Berger C *et al* 2004 Ultrathin epitaxial graphite: 2D electron gas properties and a route toward graphene-based nanoelectronics *J. Phys. Chem.* B **108** 19912

[3] Geim A K and Novoselov K S 2007 The rise of graphene *Nat. Mater.* **6** 183

[4] Castro Neto A H, Guinea F, Peres N M R, Novoselov K S and Geim A K The electronic properties of graphene *Rev. Mod. Phys.* **81** 109 (arXiv:0709.1706v2)

[5] Berger C *et al* 2006 Electronic confinement and coherence in patterned epitaxial graphene *Science* **312** 1191

[6] Emtsev K V *et al* Atmospheric pressure graphitization of SiC(0001)—a route towards wafer-size graphene layers arXiv:0808.1222

[7] Du X, Skachko I, Barker A and Andrei E Y 2008 Approaching ballistic transport in suspended graphene *Nat. Nanotechnol.* **3** 491

[8] Oshima C and Nagashima A 1997 Ultra-thin epitaxial films of graphite and hexagonal boron nitride on solid surfaces *J. Phys.: Condens. Matter* **9** 1

[9] Coraux J, N'Diaye A T, Busse C and Michely T 2008 Structural coherency of graphene on Ir(111) *Nano Lett.* **8** 565

[10] Yu Q, Lian J, Siriponglert S, Li H, Chen Y and Pei S-S 2008 Graphene segregated on Ni surfaces and transferred to insulators *Appl. Phys. Lett.* **93** 113103

[11] Nemec N, Tománek D and Cuniberti G 2006 Contact dependence of carrier injection in carbon nanotubes: an ab initio study *Phys. Rev. Lett.* **96** 076802

[12] Nemec N, Tománek D and Cuniberti G 2008 Modeling extended contacts for nanotube and graphene devices *Phys. Rev.* B **77** 125420

[13] Giovannetti G, Khomyakov P A, Brocks G, Karpan V M, van den Brink J and Kelly P J 2008 Doping graphene with metal contacts *Phys. Rev. Lett.* **101** 026803

[14] Huard B, Stander N, Sulpizio J A and Goldhaber-Gordon D 2008 Evidence of the role of contacts on the observed electron–hole asymmetry in graphene *Phys. Rev.* B **78** 121402

[15] Pletikosić I, Kralj M, Pervan P, Brako R, Coraux J, N'Diaye A T, Busse C and Michely T 2008 Weakly interacting graphene on a metal: Dirac cones and minigaps for C/Ir(111) arXiv:0807.2770

[16] Dedkov Yu S, Shikin A M, Adamchuk V K, Molodtsov S L, Laubschat C, Bauer A and Kaindl G 2001 Intercalation of copper underneath a monolayer of graphite on Ni(111) *Phys. Rev.* B **64** 035405

[17] Grüneis A and Vyalikh D V 2008 Tunable hybridization between electronic states of graphene and a metal surface *Phys. Rev.* B **77** 193401
[18] Preobrajenski A B, Ng M L, Vinogradov S and Mårtensson N 2008 Controlling graphene corrugation on lattice-mismatched substrates *Phys. Rev.* B **78** 073401
[19] Sutter P W, Flege J-I and Sutter E A 2008 Epitaxial graphene on ruthenium *Nat. Mater.* **7** 406
[20] Heersche H B, Jarillo-Herrero P, Oostinga J B, Vandersypen L M K and Morpurgo A F 2007 Bipolar supercurrent in graphene *Nature* **446** 56
[21] Dedkov Yu S, Fonin M and Laubschat C 2008 A possible source of spin-polarized electrons: the inert graphene/Ni(111) system *Appl. Phys. Lett.* **92** 052506
[22] Dedkov Yu S, Fonin M, Rüdiger U and Laubschat C 2008 Rashba effect in the graphene/Ni(111) system *Phys. Rev. Lett.* **100** 107602
[23] Karpan V M, Giovannetti G, Khomyakov P A, Talanana M, Starikov A A, Zwierzycki M, van den Brink J, Brocks G and Kelly P J 2007 Graphite and graphene as perfect spin filters *Phys. Rev. Lett.* **99** 176602
[24] Rutkov E V and Tontegode A Ya 1985 A study of the carbon adlayer on iridium *Surf. Sci.* **161** 373
[25] Marinova Ts S and Charkarov D V 1987 Adsorption of ethylene on Ir(111) *Surf. Sci.* **192** 275
[26] Marinova Ts S and Kostov K L 1987 Adsorption of acetylene and ethylene on a clean Ir(111) surface *Surf. Sci.* **181** 573
[27] N'Diaye A T, Bleikamp S, Feibelman P J and Michely T 2006 Two-dimensional Ir cluster lattices on a graphene moiré on Ir(111) *Phys. Rev. Lett.* **97** 215501
[28] N'Diaye A T, Coraux J, Plasa T, Busse C and Michely T 2008 Structure of epitaxial graphene on Ir(111) *New J. Phys.* **10** 043033
[29] Land T A, Michely T, Behm R J, Hemminger J C and Comsa G 1992 STM investigation of single layer graphite structures produced on Pt(111) by hydrocarbon decomposition *Surf. Sci.* **264** 261
[30] Ueta H, Saida M, Nakai C, Yamada Y, Sasaki M and Yamamoto S 2004 Highly oriented monolayer graphite formation on Pt(111) by a supersonic methane beam *Surf. Sci.* **560** 183
[31] Klusek Z, Kozlowski W, Waqar Z, Datta S, Burnell-Gray J S, Makarenko I V, Gall N R, Rutkov E V, Tontegode A Ya and Titkov A N 2005 Local electronic edge states of graphene layer deposited on Ir(111) surface studied by STM/CITS *Appl. Surf. Sci.* **252** 1221
[32] Marchini S, Günther S and Wintterlin J 2007 Scanning tunneling microscopy of graphene on Ru(0001) *Phys. Rev.* B **76** 075429
[33] Vásquez de Parga A L, Calleja F, Borca B, Passeggi M C G Jr, Hinarejos J J, Guinea F and Miranda R 2008 Periodically rippled graphene: growth and spatially resolved electronic structure *Phys. Rev. Lett.* **100** 056807
[34] Nieuwenhuys E, Rovida G, Hagen D I and Somorjai G A 1976 LEED AES and thermal desorption studies of chemisorbed hydrogen and hydrocarbons (C_2H_2, C_2H_4, C_6H_6, C_6H_{12}) on (111) and stepped [6(111) × (100)] iridium crystal-surfaces—comparison with platinum. *Surf. Sci.* **59** 155
[35] Land T A, Michely T, Behm R J, Hemminger J C and Comsa G 1992 Direct observation of surface reactions by scanning tunneling microscopy: ethylene → ethylidyne → carbon particles → graphite on Pt(111) *J. Chem. Phys.* **97** 6774–83
[36] Lackinger M, Greissel S, Heckel W M and Hietschold M 2002 Coronene on Ag(111) investigated by LEED and STM in UHV *J. Phys. Chem.* B **106** 4482–5
[37] Dinger A, Lutterloh C, Biener J and Küppers J 1999 Hydrogen atom reactions with graphite island edges on Pt(111) surfaces: hydrogenation through Eley–Rideal and hot-atom processes *Surf. Sci.* **421** 17
[38] Kastler M, Schmidt J, Pisula W, Sebastiani D and Müllen K 2006 From armchair to zigzag peripheries in nanographenes *J. Am. Chem. Soc.* **128** 9526
[39] La Lau C and Snyde R G 1971 A valence force field for alkyl benzenes toluene, p-xylene, m-xylene mesitylene, and some of their deuterated analogues *Spectrochim. Acta* A **27** 2073
[40] Dürr H, Kausch M and Kober H 1974 Photochemical synthesis of a tricyclo[5.4.0.$0^{1,6}$]-undecatetraene in solution *Angew. Chem. Int. Edn. Engl.* **13** 670

[41] Scott L T and Roelofs N H 1987 Thermal rearrangements of aromatic compounds. 11. Benzene ring contractions at high temperatures. evidence from the thermal interconversions of aceanthrylene, acephenanthrylene, and fluoranthene *J. Am. Chem. Soc.* **109** 5461
[42] Frenklach M and Ping J 2004 On the role of surface migration in the growth and structure of graphene layers *Carbon* **42** 1209
[43] Whitesides R, Kollias A C, Domin D, Lester W A Jr and Frenklach M 2007 Graphene layer growth: collision of migrating five-member rings *Proc. Combust. Inst.* **31** 539
[44] Rost M J, Michely T and Comsa G 1998 Comment on 'Self-diffusion and dynamic behavior of atoms at step edges on iridium surfaces' *Phys. Rev.* B **57** 1992–4
[45] Voorhees P W 1985 The theory of Ostwald ripening *J. Stat. Phys.* **38** 231
[46] Stoldt C R, Jenks C J, Thiel P A, Cadilhe A M and Evans J W 1999 Smoluchowski ripening of Ag islands on Ag(100) *J. Chem. Phys.* **111** 5157
[47] Eßer M, Morgenstern K, Rosenfeld G and Comsa G 1998 Dynamics of vacancy island coalescence on Ag(111) *Surf. Sci.* **402** 341
[48] Petersen M, Zangwill A and Ratsch C 2003 Homoepitaxial Ostwald ripening *Surf. Sci.* **536** 55–60
[49] Lee G-D, Wang C Z, Yoon E, Hwang N-M, Kim D-Y and Ho K M 2005 Diffusion, coalescence, and reconstruction of vacancy defects in graphene layers *Phys. Rev. Lett.* **95** 205501
[50] Jin C, Suenaga K and Lijima S 2008 Vacancy migrations in carbon nanotubes *Nano Lett.* **8** 1127
[51] Lee G-D, Wang C Z, Yoon E, Hwang N-M, Kim D-Y and Ho K M 2008 The formation of pentagon–heptagon pair defect by the reconstruction of vacancy defects in carbon nanotube *Appl. Phys. Lett.* **92** 043104
[52] Amara H, Bichara C and Ducastelle F 2006 Formation of carbon nanostructures on nickel surfaces: a tight-binding grand canonical Monte Carlo study *Phys. Rev.* B **73** 113404
[53] Amara H, Bichara C and Ducastelle F 2008 Understanding the nucleation mechanisms of carbon nanotubes in catalytic chemical vapor deposition *Phys. Rev. Lett.* **100** 056105
[54] Helveg S, López-Cartes C, Sehested J, Hansen P L, Clausen B S, Rostrup-Nielsen J R, Abild-Pedersen F and Nørskov J K 2004 Atomic-scale imaging of carbon nanofibre growth *Nature* **427** 426
[55] Feibelman P J 2008 Pinning of graphene to Ir(111) by flat Ir dots *Phys. Rev.* B **77** 165419
[56] Arnoult W J and McLellan R B 1972 The solubility of carbon in rhodium ruthenium iridium and rhenium *Scr. Metall.* **6** 1013
[57] Vang R T, Honkala K, Dahl S, Vestergaard E K, Schnadt J, Laegsgaard E, Clausen B S, Nørskov J K and Besenbacher F 2006 Ethylene dissociation on flat and stepped Ni(111): a combined STM and DFT study *Surf. Sci.* **600** 66
[58] Hashimoto A, Suenaga K, Gloter A, Urita K and Iijima S 2004 Direct evidence for atomic defects in graphene layers *Nature* **430** 870
[59] Suenaga K, Wakabayashi H, Koshino M, Sato Y, Urita K and Iijima S 2007 Imaging active topological defects in carbon nanotubes *Nat. Nanotechnol.* **2** 358